First observation of excited states in the $^{154}Ce_{96}$ nucleus: Rigid rotation at $Z = 58$

W. Urban,[1] T. Rząca-Urban,[1] A. G. Smith,[2] G. S. Simpson,[2] and J. P. Greene[3]

[1]*Faculty of Physics, University of Warsaw, ulica Pasteura 5, 02-093 Warsaw, Poland*
[2]*Department of Physics and Astronomy, The University of Manchester, M13 9PL Manchester, United Kingdom*
[3]*Argonne National Laboratory, Argonne, Illinois 60439, USA*

(Received 6 August 2020; accepted 8 December 2020; published 24 December 2020)

A new analysis of the data from measurements of γ radiation following spontaneous fission of ^{248}Cm and ^{252}Cf, performed using the Eurogam2 and Gammashpere arrays, respectively, has revealed, for the first time, excited states in the neutron-rich nucleus $^{154}Ce_{96}$. Using these fission data we have also improved uncertainties on γ-ray energies in the ground-state bands of several neutron-rich nuclei of the A $\approx$ 150 mass region. The improved data provided precise systematics of the $E_{exc}(4^+)/E_{exc}(2^+)$ ratio in the region, which indicate that, in the Ce isotopic chain, the rigid-rotation limit is reached at the neutron number $N = 96$, two neutrons "later" than in the chain of Nd isotopes. The new results suggest the involvement of the proton $9/2^+[404]$ extruder orbital in generating nuclear deformation in the A $\approx$ 150 region, in addition to and analogous to the known role played by the neutron $11/2^-[505]$ extruder in this region. The catalytic-type action of both extruders is discussed.

DOI: 10.1103/PhysRevC.102.064321

I. INTRODUCTION

Many decades after the discovery of strong, prolate deformation in neutron-rich nuclei of the mass A $\approx$ 150 region, the mechanism causing the sudden onset of this deformation is still not fully explained. One of the open questions concerns the change of the deformation along the proton number Z. While the evolution of the nuclear deformation along the neutron number N is rather well studied, less is known about this change along Z, especially about the low-Z limit [1] of the A $\approx$ 150 deformation region.

As demonstrated by Sharpey-Schaffer *et al.* in their recent review [2], backed by other studies [3–6], the $11/2^-[505]$ neutron extruder orbital, originating from the $h_{11/2}$ shell, plays an essential role in generating nuclear deformation in the A $\approx$ 150 region. This upsloping Nilsson state, nicknamed "flying-fish" in Ref. [2], acts as a kind of catalyst, helping nuclei to deform.

Such a role of an extruder is also supported by studies of mass A $\approx$ 100, neutron-rich nuclei, another place where strong nuclear deformation was found [7]. The sudden onset of the deformation at the neutron number N $\approx$ 60 [8–10] was explained as due to the $9/2^+[404]$ neutron extruder orbital [11], observed at the Fermi surface in this region [12–15]. One may ask if the $9/2^+[404]$ *proton* extruder could play a role in generating nuclear deformation in the mass A $\approx$ 150 neutron-rich nuclei and in defining the low-Z limit of this deformation region.

In the present work we report on the first observation of excited states in the neutron-rich nucleus, $^{154}_{58}Ce_{96}$. The new data indicate that the rigid-rotation limit is reached in this nucleus, moving the low-Z limit of the A $\approx$ 150 deformation region down to 58 protons. A possible role of the $9/2^+[404]$ proton extruder in the deformation process is discussed. In Sec. II we describe the experiment and the new experimental data, which are then discussed in Sec. III. The paper is summarized in Sec. IV.

II. EXPERIMENT AND RESULTS

New information on the ^{154}Ce nucleus has been obtained from measurements of γ rays following spontaneous fission of ^{248}Cm and ^{252}Cf, performed using the Eurogam2 [16] and Gammasphere [17] arrays, respectively. Both experiments were described previously [18–20]. The progress in computing technologies and analysis techniques allowed an improved reevaluation (higher-resolution sorting, energy calibrations with a constant peak width, background reduction) of these data, revealing weak effects not noticed at earlier stages of the analysis, among others, the observation of γ transitions in ^{154}Ce. The use of both ^{248}Cm and ^{252}Cf fission data provided the countercheck of the results.

Figure 1 shows the partial excitation scheme of ^{154}Ce obtained in this work. The scheme comprises four γ transitions, corresponding to new γ lines found in coincidence spectra gated on γ lines of the ^{92}Sr nucleus (in ^{248}Cm fission data) and on γ lines of the ^{96}Zr nucleus (in ^{252}Cf fission data). Energies of new γ lines with their uncertainties are shown in the scheme. The transitions are arranged into one cascade, based on their mutual coincidence relations. Their order in the cascade is based on relative γ intensities, shown in square brackets, and on their energies. It is proposed that they form a rotational band with energies growing with spin [21]. Figure 2(a) displays the low-energy part of the coincidence γ spectrum, showing the 76.3-keV line assigned to ^{154}Ce. The spectrum is a sum of two spectra doubly gated on the 176.0–

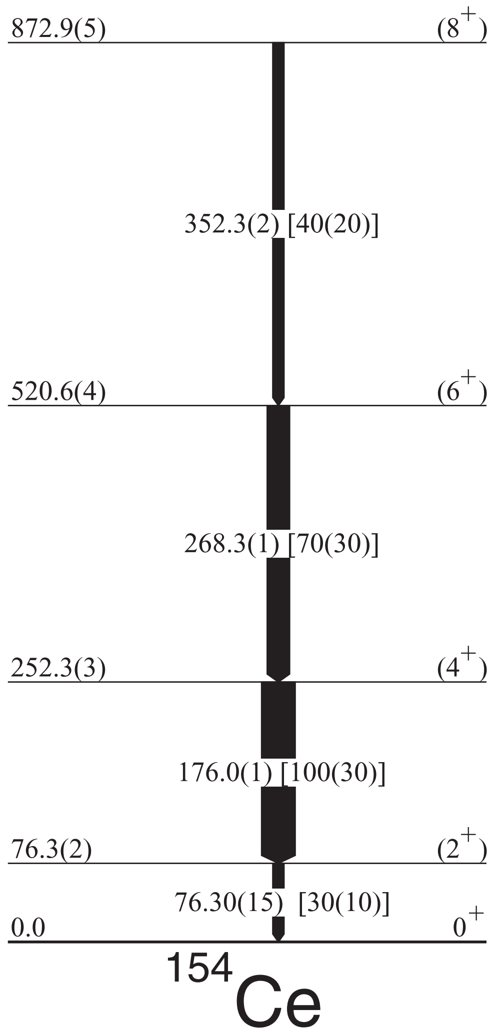

FIG. 1. Partial level scheme of ^{154}Ce, as obtained in this work.

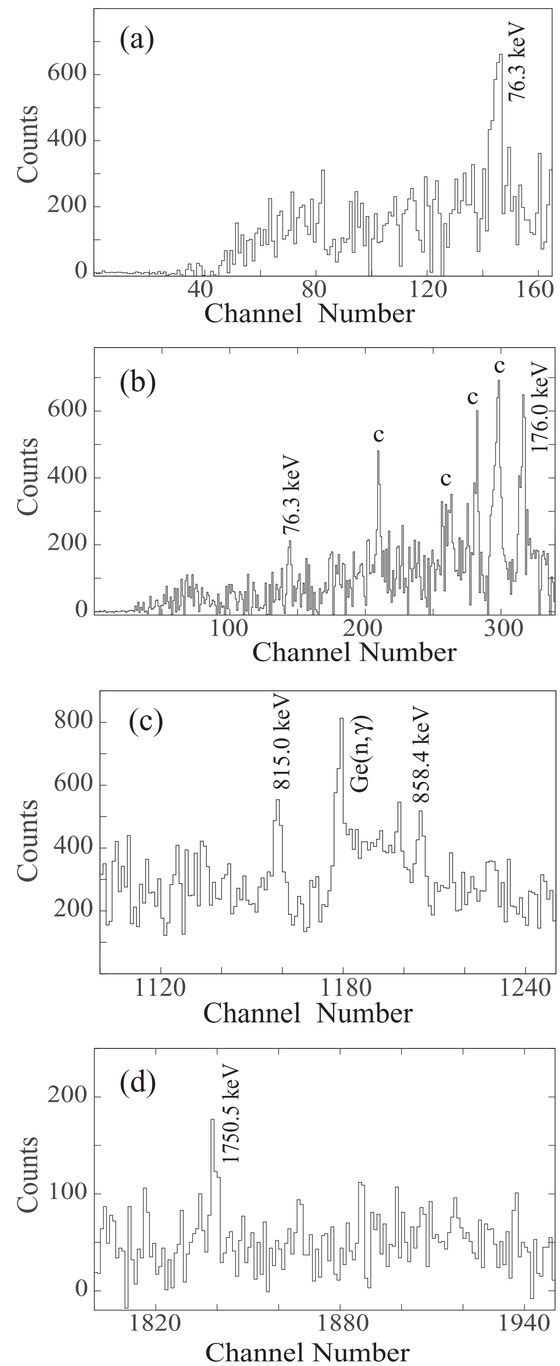

FIG. 2. Coincidence spectra gated on transitions assigned to ^{154}Ce and on transitions in complementary fission fragments, as seen in this work. Coefficients for the quadratic energy calibration of the spectra, $E_\gamma\,(\mathrm{keV}) = \mathrm{A}_0 + \mathrm{A}_1 \times \mathrm{channel} + \mathrm{A}_2 \times \mathrm{channel}^2$, are $\mathrm{A}_0 = 0.49$, $\mathrm{A}_1 = 0.498\,808\,1$ and $\mathrm{A}_2 = 0.000\,177\,204$ for the ^{248}Cm fission data and $\mathrm{A}_0 = 0.11$, $\mathrm{A}_1 = 0.666\,750\,0$ and $\mathrm{A}_2 = 0.000\,155\,175$ for the ^{252}Cf fission data. Note the large A_2 values of these "constant-peak-width" calibrations. The label "c" denotes contaminating γ lines. See text for more comments.

268.3-keV and 176.0–352.3-keV lines, using ^{248}Cm-fission data. Figure 2(b) displays the low-energy part of the coincidence γ spectrum, showing the 76.3- and 176.0-keV lines assigned to ^{154}Ce. The spectrum is doubly gated on the 268.3- and 352.3-keV lines using ^{248}Cm-fission data (the 352-keV line, present in a number of other nuclei populated in fission, is responsible for the contaminating peaks in the spectrum).

The assignment of γ transitions shown in Fig. 1 to the ^{154}Ce nucleus was done based on two observations:

(i) The transitions were assigned to a cerium isotope, based on the observed cross coincidences between these γ rays and the known γ rays in the complementary fission fragments, which are isotopes of strontium in fission of ^{248}Cm and isotopes of zirconium in fission of ^{252}Cf. Figure 2(c) displays a fragment of a sum of two γ spectra doubly gated on the 176.0–268.3-keV and 176.0–352.3-keV lines in the ^{248}Cm fission data. The spectrum shows the known 815.0- and 858.4-keV γ lines of ^{92}Sr. The same gating performed using ^{252}Cf fission data provided a spectrum, a fragment of which is shown in Fig. 2(d), where the 1750.5-keV line is seen, corresponding to the ground-state transition

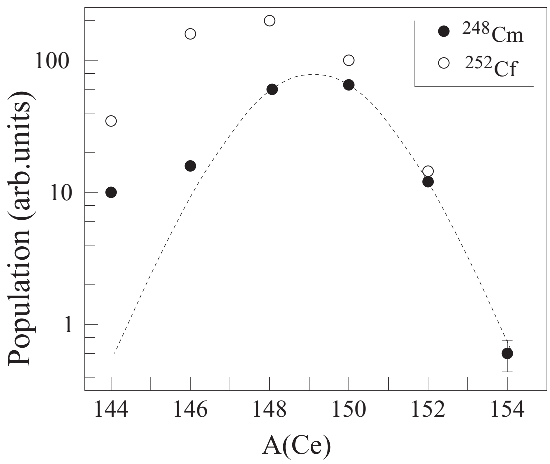

FIG. 3. Population (in arbitrary units) of even-even Ce isotopes in spontaneous fission of ^{248}Cm (filled circles) and in spontaneous fission of ^{252}Cf (empty circles). The dashed line represents the Gaussian distribution (see formula in the text), fit to the data points for ^{148}Ce, ^{150}Ce, and ^{152}Ce isotopes, populated in fission of ^{248}Cm.

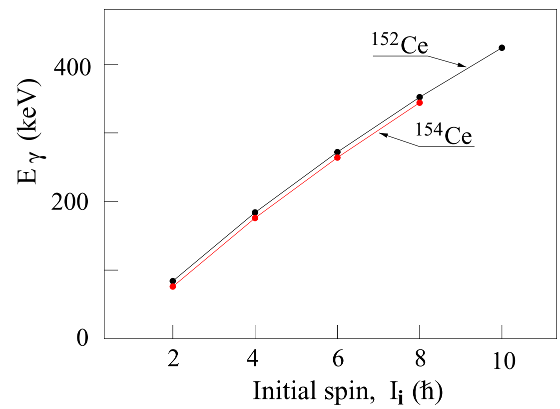

FIG. 4. Energies of γ transitions, E_γ, in ground-state cascades of ^{152}Ce and ^{154}Ce, as a function of the initial spin I_i. The data for ^{152}Ce were taken from Ref. [25].

in ^{96}Zr. The data in Fig. 2 indicate that the newly identified cascade belongs to an isotope of cerium.

(ii) To assign the new cascade to a particular cerium isotope, we estimated triple-γ coincidence intensities (corrected for γ efficiency of Ge arrays and for the internal-conversion effect) in the 6^+-4^+-2^+-0^+ ground-state cascades of even-even Ce isotopes seen in ^{248}Cm fission data. It is expected that these intensities are proportional to the population of cerium isotopes in the spontaneous fission of ^{248}Cm. The intensities obtained for cascades of known $^{144–152}$Ce isotopes and the intensity in the new 76.3-176.0-268.3-keV cascade are shown in Fig. 3 as filled circles, using arbitrary units proportional to the triple-γ intensities. The uncertainties of the data points in the $A = 144$–152 range are smaller than sizes of the circles. To the data points corresponding to ^{148}Ce, ^{150}Ce, and ^{152}Ce we fit the Gaussian distribution

$$P(A) = C\, e^{\left[-\frac{(A-A_0)^2}{2\sigma^2}\right]}, \qquad (1)$$

where A denotes mass number and $\sigma = 1.6$ was taken from systematics [22]. $A_0 = 148.1$ and the normalization factor C were adjusted to the three points. The triple-γ intensity of the new cascade fits well that expected for ^{154}Ce. A similar Gaussian distribution, with the same width σ was observed for even-even Ba isotopes in the same ^{248}Cm fission data (see Fig. 2 in Ref. [23]).

In Fig. 3 one sees at $A = 144$ (and to a lower extent at $A = 146$) the know effect of the cumulative yield due to β^- decay in isobaric chains of fission fragments (the high triple-γ intensity due to the cumulative yield in ^{144}Ce, resulting from β^- decay of the ^{144}La ground state with spin $I = 3$, enabled recent detailed study of ^{144}Ce [24]). In Fig. 3 we also show the population of Ce isotopes in the ^{252}Cf-fission data, using in the same arbitrary units. Although the statistics of the ^{252}Cf-fission measurement is higher, the population of ^{154}Ce is comparable to that in ^{248}Cm-fission measurement because the ^{248}Cm fission has the maximum of the population at slightly higher neutron number compared with the ^{252}Cf fission. The higher cumulative yield in ^{252}Cf-fission data is due the longer coincidence-time window in the ^{252}Cf measurement, as compared with the ^{248}Cm measurement. The 76.3-166.0-268.3-keV coincidence in the ^{252}Cf data is contaminated and is not shown in Fig. 3.

The assignment of the new cascade to ^{154}Ce is further supported by the similarity between this cascade and the ground-state cascade of ^{152}Ce, as illustrated in Fig. 4, which shows energies of the γ transition in these cascades, as a function of spins of the respective initial levels.

The expected data point at $A = 150$ in the intensity distribution of Ba isotopes shown in Fig. 2 of Ref. [23] suggests that ^{150}Ba may be observed in fission of ^{248}Cm, considering that this fission source is very efficient in populating neutron-rich isotopes as compared with other sources [26]. The ^{150}Ba nucleus was not found in Ref. [23] but with the improved analysis techniques it was possible to see it in the present work. This observation was helped by the recent identification of this nucleus in Ref. [27] and is the first confirmation of this exotic data. In the present work we could observe one more transition in the ground-state cascade of ^{150}Ba, as listed in Table I.

High-precision measurements of γ transition energies are essential for tracing the evolution of nuclear deformation in nuclei past the $N = 90$ line, where differences between ground-state cascades become minute. Very useful in such analysis is the ratio of the first two excitation energies in the ground-state bands, $R_{4/2} = E_{\rm exc}(4^+)/E_{\rm exc}(2^+)$. With precise $R_{4/2}$ values one may follow small but meaningful variances in the deformation. Such high-precision data are used, for example, in testing the confined β-soft (CBS) rotor model [28], reproducing rotational cascades in the A $\approx$ 150 region with the relative accuracy of about 10^{-3} [29]. We note that, at present, γ-ray energy measurements are the unique source of sufficiently precise experimental data for testing the high-

TABLE I. Energies E_γ of γ lines corresponding to $E2$ transition in ground-state cascades of even-even nuclei from mass A ≈ 150 region, (a) observed in this work, and (b) compared with literature values taken from Refs. [27,30–32]. See text for more comments.

Spin I_i	E_γ [a] (keV)	E_γ [b] (keV)
	^{140}Xe	
2	376.65(5)	376.66(2)
4	457.68(5)	457.63(2)
6	582.47(5)	582.44(5)
8	566.55(5)	566.64(5)
	^{142}Xe	
2	287.18(5)	287.2(2)
4	403.44(5)	403.5(2)
6	490.38(5)	490.4(2)
8	551.30(5)	551.1(2)
	^{144}Xe	
2	252.42(5)	252.6
4	391.85(5)	391.7
6	487.75(5)	487.9
8	555.75(5)	555.8
	^{142}Ba	
2	359.57(5)	359.598(14)
4	475.15(5)	475.15(5)
6	631.40(5)	631.25(5)
8	693.55(5)	693.55(5)
	^{144}Ba	
2	199.32(5)	199.33(1)
4	330.90(5)	330.88(9)
6	431.40(5)	431.3(1)
8	509.40(5)	509.3(1)
	^{146}Ba	
2	181.15(5)	181.04(5)
4	332.60(5)	332.44(13)
6	444.80(5)	444.70(10)
8	524.30(5)	524.29(5)
	^{148}Ba	
2	141.76(5)	141.8(1)
4	281.36(5)	281.3(1)
6	385.00(5)	384.8(1)
8	456.95(5)	456.8(1)
	^{150}Ba	
2	101.13(22)	101.1(1)
4	217.05(7)	217.1(2)
6	332.1(1)	
	^{146}Ce	
2	258.53(5)	258.43(5)
4	409.90(5)	409.78(5)
6	503.10(5)	503.0(1)
8	565.65(5)	565.60(16)
	^{148}Ce	
2	158.50(5)	158.468(5)
4	295.12(5)	295.07(9)
6	386.30(5)	386.15(20)
8	451.07(5)	450.75(20)
	^{150}Ce	
2	97.10(5)	97.0(1)
4	208.90(5)	208.7(2)
6	300.60(5)	300.7
8	376.15(5)	376.2

TABLE I. (*Continued*).

Spin I_i	E_γ [a] (keV)	E_γ [b] (keV)
	^{152}Ce	
2	80.95(5)	81.2(5)
4	182.70(5)	182.8(5)
6	274.42(5)	274.6(5)
8	355.35(5)	355.6
	^{150}Nd	
2	130.22(5)	130.22(9)
4	250.25(5)	251.24(9)
6	339.00(5)	339.1(5)
8	409.25(5)	409.5(5)
	^{152}Nd	
2	72.70(5)	72.41(5)
4	164.10(5)	164.11(6)
6	247.15(5)	247.43(11)
8	321.95(5)	322.2
	^{154}Nd	
2	70.82(5)	70.8(1)
4	162.50(5)	162.4(1)
6	248.50(5)	248.6
8	327.95(5)	328.2
	^{156}Nd	
2	67.3(1)	67.2(2)
4	155.00(5)	155.0(2)
6	238.70(5)	238.6(2)
8	317.50(5)	317.5(2)
	^{156}Sm	
2	75.75(5)	75.88(5)
4	174.12(5)	173.75(5)
6	267.37(5)	267.32(5)
8	354.65(5)	354.5(2)
	^{158}Sm	
2	72.65(8)	72.8(1)
4	167.40(5)	167.5(1)
6	258.30(5)	258.1(1)
8	344.15(5)	344.0(2)
	^{160}Sm	
2	70.70(5)	70.9(2)
4	162.15(5)	162.4(2)
6	250.00(5)	250.4(2)
8	333.25(5)	333.5(2)
	^{160}Gd	
2	75.70(20)	75.26(1)
4	173.86(5)	173.19(9)
6	267.10(5)	266.31(8)
8	353.15(5)	353.19(9)
	^{162}Gd	
2	71.55(15)	71.6
4	165.00(5)	164.8
6	253.55(5)	253.6
8	336.20(5)	336.2
	^{164}Gd	
2	73.35(20)	73.27(5)
4	168.10(7)	168.4(4)
6	261.15(8)	261.3
8	349.10(0)	349.0

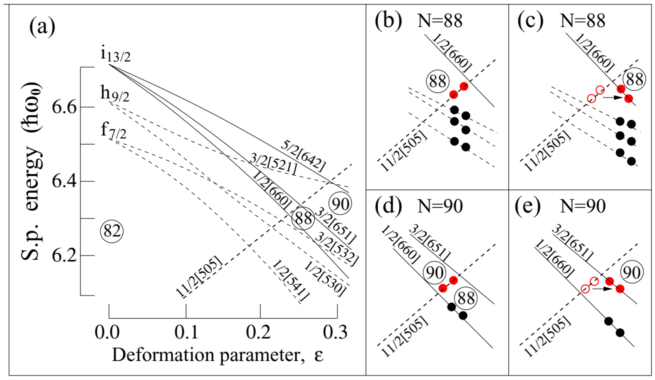

FIG. 5. (a) Nilsson diagram for neutrons, sketched after Ref. [33]. (b)–(e) Schematic drawings of fragments of the Nilsson diagram for neutrons. Filled and empty circles represent neutron particles and holes, respectively. See text for more comments.

accuracy predictions of the CBS calculations, essential for modeling the centrifugal stretching [28,29].

To help the discussion of the deformation in ^{154}Ce and other nuclei in the region, using the $R_{4/2}$ ratio, we improved uncertainties in ground-state cascades of several nuclei, as listed in Table I. This was possible due to the improved energy calibrations in our ^{248}Cm and ^{252}Cf fission-data sets (enabled, among others, by the increased precision of γ transition energies in fission fragments reported in the database Ref. [30] for ^{140}Xe, ^{142}Ba, ^{144}Ba, ^{146}Ba, ^{146}Ce, ^{148}Ce, ^{152}Nd, and ^{156}Sm). One may notice rather good agreement of our energies with the literature values, although there are also some differences, for example, in ^{160}Gd. Further in the text we use, where available, the γ energies and their uncertainties as determined in this work. The uncertainties of individual energy calibrations for our ^{248}Cm and ^{252}Cf data sets are about 0.03 keV in the energy range from 50 keV to 1 MeV, while the differences between the two calibrations are less than 0.05 keV. Therefore, for the transitions listed in Table I with statistical uncertainties smaller than 0.05 keV, we adopted the uncertainty of 0.05 keV.

It can be seen that, for many transitions listed in Table I, their uncertainties are either significantly improved (as in ^{152}Ce) or reported for the first time (as in ^{144}Xe and ^{162}Gd). In Table I we also included transitions depopulating levels with spins $I = 6$ and $I = 8$, used in analyses of $R_{6/2}$ and $R_{8/2}$ ratios. For the ^{160}Gd isotope our γ energies differ from the literature values, although the resulting $R_{4/2}$ values are the same, within uncertainties. Here we used the $R_{4/2}$ value calculated using the more precise literature γ energies. As commented in Ref. [30], some of the γ energies, not available originally, were estimated by the evaluators.

III. DISCUSSION

As shown in Ref. [2] and discussed below, the $11/2^-[505]$ neutron Nilsson orbital plays an important, multiple role in generating nuclear deformation and shape coexistence in the A ≈ 150 region, acting as a kind of catalyst for the two phenomena. The relevant fragment of the Nilsson diagram for the region, drawn after Ref. [33], is shown in Fig. 5(a) to help the discussion.

Once the $1/2^-[541]$, $1/2^-[530]$, and $3/2^-[532]$ low-Ω, neutron orbitals of the $f_{7/2}$ and $h_{9/2}$ parentage are filled, which gradually increases the deformation to a value just above $\epsilon = 0.2$, the $11/2^-[505]$ orbital extrudes from below the $N = 82$ shell gap, approaching the Fermi level and delivering two extra neutrons to the valence space, as sketched in Fig. 5(b). Thus, there are effectively eight valence nucleons at $N = 88$, as compared with four valence neutrons at $N = 86$. This sudden increase of active neutrons is one of the reasons for a quick rise of nuclear deformation at $N = 88$ in the A ≈ 150 neutron-rich nuclei.

Furthermore, the extra pair of neutrons may be shifted from the $11/2^-[505]$ extruder to the downsloping, $1/2^+[660]$, Nilsson orbital, originating from the $i_{13/2}$ neutron shell as sketched in Fig. 5(c). The population of the deformation-driving, $1/2^+[660]$ intruder accompanied by vacating the spherical-driving, $11/2^-[505]$ extruder contributes further to the sudden increase of deformation in this region, a mechanism proposed long ago [34,35]. The shift of the neutron pair proceeds via the neutron-pair hopping at the crossing of the extruder with the intruder, as depicted in the "pair-hopping" model [36,37] (see Fig. 1 in Ref. [37]) and commented in the review paper by Matsuyanagi *et al.* [38]).

The $11/2^-[505]$ extruder, delivering a pair of neutrons to the Fermi level [Fig. 5(b)] and then passing this pair to the $1/2^+[660]$ intruder [Fig. 5(c)] participates in creating at $N = 88$ a low-lying, $I^\pi = 0_2^+$ level coexisting with the 0_1^+ ground state. Such coexistence is commonly observed in the A ≈ 150 region [39–41] but which of the two 0^+ levels is more deformed is not obvious [11,42]. It depends on the details of single-particle excitations and residual interactions determining the Fermi level, and cannot be judged from schematic diagrams, as shown in Fig. 5. Furthermore, it was pointed out that some changes to the standard Nilsson scheme are in order due to the evolution of spin-orbit interactions at high neutron excess [43–45]. A dedicated calculation in this region, performed for the neodymium isotopes, shows a significant variation of the Fermi level with the increasing neutron number, apparently lowering in the 82 < N < 94 range [46] (it also shows that energies of neutron single-particle levels differ from the standard scheme of Ref. [33]).

As seen in Fig. 5, around $N = 90$ the $11/2^-[505]$ extruder crosses a number of intruder orbitals, which appear in close proximity at the Fermi level. Therefore its action in the region is not limited to passing just one pair of neutrons, as shown in Figs. 5(b) and 5(c). Rather, when going two neutrons up from $N = 88$, the extruder acquires another pair of neutrons, as shown in Fig. 5(d), which is then passed to the next, $3/2^+[651]$ intruder orbital, as illustrated in Fig. 5(e). This increases further the deformation, compared with $N = 88$, and creates close-lying 0_1^+ and 0_2^+ configurations at $N = 90$. The Nilsson scheme in Fig. 5(a) suggests that this catalytic-type action involves more of such crossings in the A ≈ 150 region. This corresponds well to the observed range of the sudden change of nuclear deformation, extending from $N = 88$ to $N = 92$, accompanied by the coexistence of 0_1^+ ground-state configurations with the low-lying, excited 0_2^+ configurations

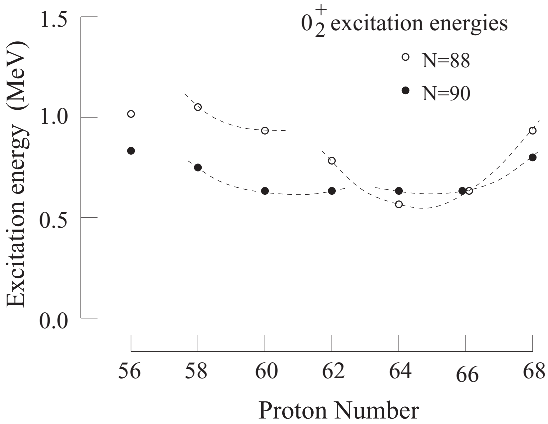

FIG. 6. Systematics of 0_2^+ excitation energies in the $N = 88$ and $N = 90$ isotones of the A ≈ 150 region. Dashed lines are drawn to guide the eye. See text for more comments.

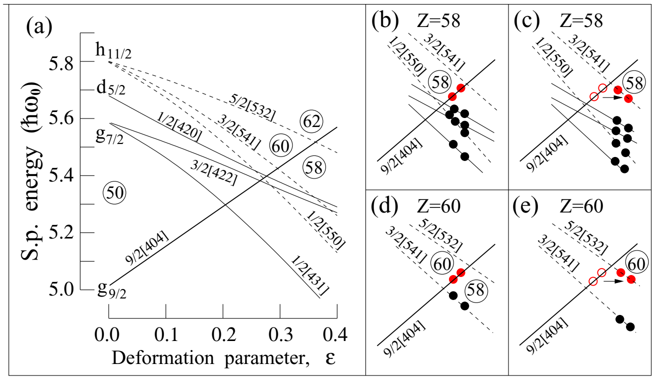

FIG. 7. Schematic Nilsson diagram for protons. Filled and empty circles represent proton particles and holes, respectively. See text for further comments.

in this neutron range. A strong correlation between the 0_2^+ configurations and the position of the $11/2^-[505]$ extruder relative to the Fermi level can be seen in Fig. 11 of Ref. [2] and in Fig. 5 of Ref. [47].

Figure 6 displays excitation energies of the 0_2^+ excitations in the A ≈ 150 neutron-rich nuclei, shown as a function of proton number Z for the $N = 88$ and $N = 90$ isotones, in which these energies have the lowest values in the region. One sees here an interesting variation of 0_2^+ excitation energy, which goes down at $Z = 58$ and rises again at $Z = 68$. Moreover, the proton range, where 0_2^+ excitations are lowest, depends on the neutron number N. In $N = 90$ isotones this is seen from Ce to Dy nuclei, where the energies are nearly constant. At $N = 88$, the lowest values are observed at higher proton number in Sm, Gd, and Dy nuclei. The systematics suggests that the $58 \leqslant Z \leqslant 66$ range splits into two smaller regions of four to six protons.

The limited range of protons where the low-lying 0_2^+ levels appear is analogous to the limited range of neutrons, where one observes the involvement of the $11/2^-[505]$ neutron extruder (Fig. 11 of Ref. [2]). One may then ask whether the $9/2^+[404]$ *proton* extruder plays any role in generating nuclear deformation in A ≈ 150 neutron-rich nuclei, in addition to the action of the $11/2^-[505]$ neutron extruder. The answer is not obvious because protons, which are more strongly bound than neutrons in this region, may respond differently to nuclear deformation than neutrons. This can be seen in Fig. 7(a), showing the relevant fragment of the Nilsson diagram for protons above the $Z = 50$ shell. One notices that the $9/2^+[404]$ proton extruder crosses the low-Ω intruders of the $h_{11/2}$ parentage at higher deformation, ϵ, as compared with analogous crossings in the neutron diagram in Fig. 5(a).

The $9/2^+[404]$ proton extruder has not been directly observed in the odd-Z, A ≈ 150 neutron-rich nuclei to date. Therefore the type of correlation, as shown in Fig. 11 of Ref. [2], is not yet available to demonstrate its contribution to the shape change and shape coexistence in this region. Instead, we examine in more detail the deformation of even-even nuclei of the region in terms of the $R_{4/2} = E_{\mathrm{exc}}(4^+)/E_{\mathrm{exc}}(2^+)$ energy ratio, to search for possible signs of the $9/2^+[404]$ proton extruder influence on nuclear deformation, analogous to the effects caused by the $11/2^-[505]$ neutron extruder.

In Fig. 8 we show the $R_{4/2}$ ratio for Ba–Dy isotopes as a function of neutron number N. The scale of the figure is strongly expanded to show various effects, as discussed below. The uncertainties of the data points, if not drawn, are lower than the size of the data symbols. The tables inserted in Fig. 8 list the $R_{4/2}$ values with uncertainties, as obtained from the data listed in Table I and reported in Ref. [30].

The most prominent feature seen in Fig. 8 is the rapid increase of the deformation between $N = 90$ and $N = 92$,

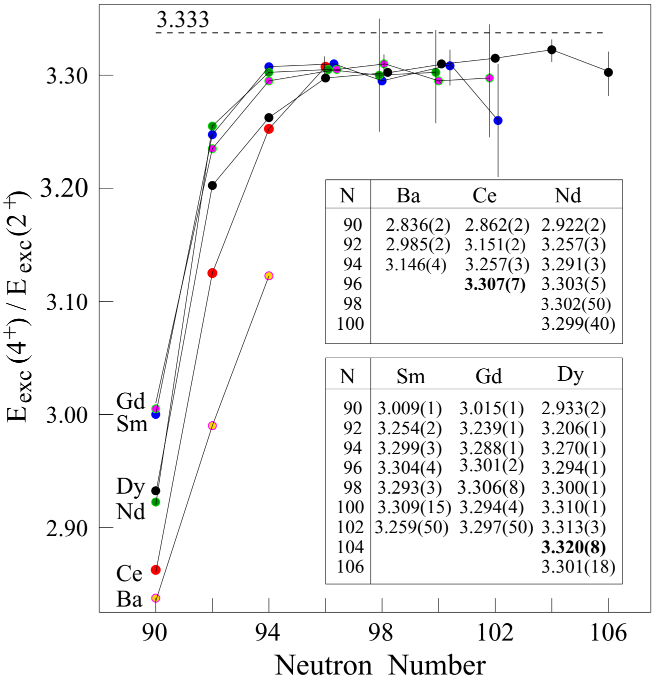

N	Ba	Ce	Nd
90	2.836(2)	2.862(2)	2.922(2)
92	2.985(2)	3.151(2)	3.257(3)
94	3.146(4)	3.257(3)	3.291(3)
96		**3.307(7)**	3.303(5)
98			3.302(50)
100			3.299(40)

N	Sm	Gd	Dy
90	3.009(1)	3.015(1)	2.933(2)
92	3.254(2)	3.239(1)	3.206(1)
94	3.299(3)	3.288(1)	3.270(1)
96	3.304(4)	3.301(2)	3.294(1)
98	3.293(3)	3.306(8)	3.300(1)
100	3.309(15)	3.294(4)	3.310(1)
102	3.259(50)	3.297(50)	3.313(3)
104			**3.320(8)**
106			3.301(18)

FIG. 8. $E(4^+)/E(2^+)$ ratio as a function of the neutron number. Inset tables show the $R_{4/2}$ ratio calculated using data from Table I. For Dy isotopes the data are taken from Ref. [30]. See text for more comments.

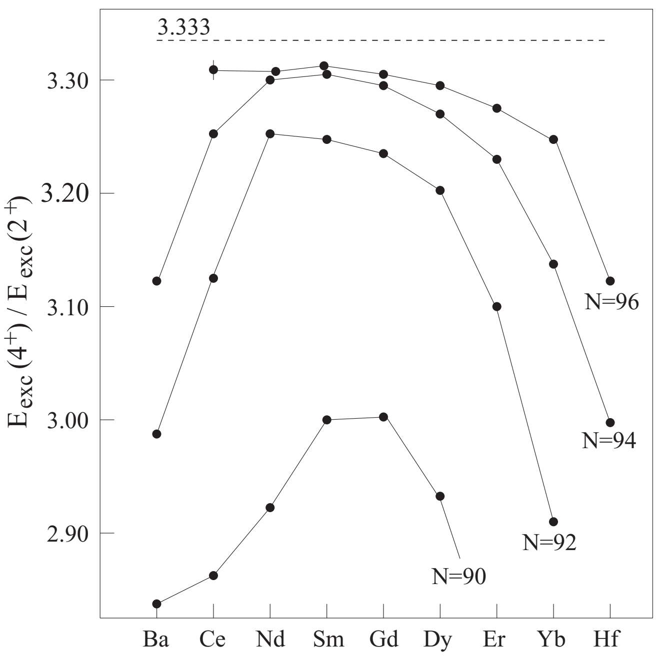

FIG. 9. $E(4^+)/E(2^+)$ ratio as a function of proton number. See text for more explanation.

where the $R_{4/2}$ ratio increases by about 0.3 per pair of neutrons added. A similarly rapid increase is observed between $N = 88$ and $N = 90$ (not shown in Fig. 8). Above $N = 92$ the deformation grows slower, saturating above $N = 94$. This reflects the catalytic action of the $11/2^-[505]$ neutron extruder in the $88 \leqslant N \leqslant 92$ range, as described above.

Figure 9 displays the $R_{4/2}$ ratio for the $N = 90$ to $N = 96$ isotones in the region as a function of the proton number Z in a range from $Z = 56$ (Ba) to $Z = 72$ (Hf). As in Fig. 8, uncertainties of the data points, if not drawn, are less than the size of the data symbols. In the figure one observes a rapid increase of deformation between Ba and Nd. Although the rise of about 0.15 per pair of protons added is slower than in Fig. 8, the effect is clear, especially in the $N = 92$ isotones, where the deformation increases quickly up to ^{152}Nd and then stops growing.

This observation suggests that there may be a catalytic action of the $9/2^+[404]$ proton extruder in the process of the deformation change in the A $\approx$ 150 region, analogous to the action of the $11/2^-[505]$ neutron extruder. This is sketched in Fig. 7(b), where the $9/2^+[404]$ proton extruder delivers two extra protons to the Fermi level, increasing the number of active valence protons to 10, already at $Z = 58$. This coincides with the faster increase of deformation in Ce isotopes than in Ba isotopes, seen in Fig. 8. The extra proton pair may then be passed to the $3/2^-[541]$ proton intruder, increasing the deformation (which is further helped by vacating the $9/2^+[404]$ proton extruder) and creating another 0^+ configuration at $N = 58$, as sketched in Fig. 7(c). This action is continued at the next proton extruder-intruder crossing, as sketched in Figs. 7(d) and 7(e).

While the above scenario seems plausible, it needs extra comments. In the case of neutrons, the rapid increase in deformation is well correlated in neutron number with the appearance of low-lying 0_2^+ excitations strongly supporting the catalytic role of the $11/2^-[505]$ extruder in the process. Analogous correlation is less clear in the case of protons. As seen in Fig. 6, the lowest 0_2^+ configurations appear at $N = 88$ and $N = 90$ while Fig. 9 suggest that, in N < 90 isotones, there is no involvement of the $9/2^+[404]$ proton extruder in the deformation increase. One may, therefore, conclude that the low-lying 0_2^+ excitations at $N = 88$ and $N = 90$ involve, primarily, the $11/2^-[505]$ neutron extruder, which also plays the main role in the deformation change at $N \leqslant 90$.

The $9/2^+[404]$ proton extruder is likely to be involved in the deformation increase at N > 90, only. This reflects the fact that, while the extruder helps in the deformation change, the deformation itself is, primarily, a proton-neutron effect [48], which is governed by the $N_\pi \times N_\nu$ product of valence protons and neutrons [49]. Therefore, with the $9/2^+[404]$ proton extruder active at $Z = 58$ (see Fig. 7) it takes two more neutrons to reach rigid rotation in ^{154}Ce, compared with ^{154}Nd, as seen in Fig. 9. One may expect that, at N > 96, the rigid rotation limit will be reached in the barium isotopic chain, considering possible involvement of the $9/2^+[404]$ proton extruder already at $Z = 56$, as suggested by Fig. 7. Because nuclear deformation influences β^--decay half-lives, such information should be important for tracing the r-process path [50], a subject of intensive studies in the A $\approx$ 150 region [51–53].

The new $R_{4/2} = 3.307(7)$ ratio obtained for ^{154}Ce strengthens the observation that this ratio never reaches the 3.333 limit. The top twenty values shown in Fig. 8 appear within the 3.301(13) range [the highest value of 3.320(8) in the region, observed in ^{170}Dy, is in the limit within its uncertainty). This suppression is explained as the effect of the centrifugal stretching, described and precisely reproduced within the confined β-soft rotor model [29]. Using such data one can probe the elasticity of the nuclear matter and, in particular, the stiffness of the nuclear potential in the β direction. This may provide new information on the microscopic nature of the confined β-soft potential, contributing to the understanding of the enigmatic "β-vibrations" [2,40]. We stress here the need for high-precision measurements of γ energies. As seen in Fig. 8, the data points with uncertainties $\Delta R > 0.015$ are less useful.

IV. SUMMARY

In summary, an improved analysis of multiple-γ coincidences from measurements of γ rays following spontaneous fission of ^{248}Cm and ^{252}Cf performed with the Eurogam2 and Gammasphere arrays allowed the first observation of excited states in the very-neutron-rich nucleus ^{154}Ce. We also confirmed and extended the ground-state cascade of another very-neutron-rich nucleus ^{150}Ba and improved uncertainties on γ energies in ground-state cascades of twenty other nuclei in the A $\approx$ 150 region.

Analysis of the $R_{4/2} = E(4^+)/E(2^+)$ ratio, calculated using the improved energies, suggest that, in the very-neutron-rich isotopes of the A $\approx$ 150 region, the $9/2^+[404]$ proton extruder orbital plays a role in the sudden nuclear deformation onset, in addition to and analogous to the catalytic-type action of the $11/2^-[505]$ neutron extruder, recognized previously.

Furthermore, the analysis firmly moves the low-Z limit of the A $\approx$ 150 deformation region down to $Z = 58$ and suggests that this limit may be shifted further down, to $Z = 56$, at the neutron number $N > 96$.

The present work demonstrates the importance of high-precision measurements of γ-ray energies for testing the mechanism and the limits of nuclear deformation as well as the nature of the disputed "β vibrations."

ACKNOWLEDGMENTS

This material is based upon work supported by the U.S. Department of Energy, Office of Science, Office of Nuclear Physics, under Contract No. 1 DE-AC02-06CH11357. The authors are indebted for the use of ^{248}Cm to the Office of Basic Energy Science, U.S. Department of Energy, through the transplutonium element production facilities at the Oak Ridge National Laboratory.

[1] P. Koseoglou, V. Werner, N. Pietralla, S. Ilieva, T. Niksić, D. Vretenar, M. Thürauf, C. Bernards, A. Blanc, A. M. Bruce, R. B. Cakirli, N. Cooper, L. M. Fraile, G. de France, M. Jentschel, J. Jolie, U. Köster, W. Korten, T. Kröll, S. Lalkovski *et al.*, Phys. Rev. C **101**, 014303 (2020).

[2] J. F. Sharpey-Schafer, R. A. Bark, S. P. Bvumbi, T. R. S. Dinoko, and S. N. T. Majola, Eur. Phys. J. A **55**, 15 (2019).

[3] J. F. Sharpey-Schafer, S. M. Mullins, R. A. Bark, J. Kau, F. Komati, E. A. Lawrie, J. J. Lawrie, T. E. Madiba, P. Maine. A. Minkova, S. H. T. Murray, N. J. Ncapayi, and P. A. Vymers, Eur. Phys. J. A **47**, 5 (2011).

[4] J. F. Sharpey-Schafer, T. E. Madiba, S. P. Bvumbi, E. A. Lawrie, J. J. Lawrie, A. Minkova, S. M. Mullins, P. Papka, D. G. Roux, and J. Timar, Eur. Phys. J. A **47**, 6 (2011).

[5] S. N. T. Majola, M. A. Sithole, L. Mdletshe, D. Hartley, J. Timar, B. M. Nyakó, J. M. Almond, R. A. Bark, C. Beausang, L. Bianco, T. D. Bucher, S. P. Bvumbi, M. P. Carpenter, C. J. Chiara, N. Coope, D. M. Cullen, D. Curien, T. S. Dinokio, B. J. P. Gall, P. E. Garrett *et al.*, Phys. Rev. C **101**, 044312 (2020).

[6] M. A. Sithole, J. F. Sharpey-Schafer, S. N. T. Majola, T. D. Bucher, T. R. S. Dinokio, S. S. Ntshangase, E. A. Lawrie, N. A. Khumalo, S. Jongile, L. Mdletshe, R. A. Bark, N. Erasmus, P. Jones, B. V. Khesva, J. J. Lawrie, L. Makhathini, K. L. Malatji, B. Maqabuka, S. P. Noncolela, J. Ndayishimye *et al.*, Eur. Phys. J. A **55**, 178 (2019).

[7] E. Chiefetz, R. C. Jared, S. G. Thompson, and J. B. Wilhelmy, Phys. Rev. Lett. **25**, 38 (1970).

[8] R. K. Sheline, I. Ragnarsson, and G. Nilsson, Phys. Lett. B **41**, 115 (1972).

[9] G. Lhersonneau, B. Pfeiffer, K.-L. Kratz, T. Enqvist, P. P. Jauho, A. Jokinen, J. Kantele, M. Leino, J. M. Parmonen, H. Penttilä, and J. Äystö, Phys. Rev. C **49**, 1379 (1994).

[10] W. Urban, J. L. Durell, A. G. Smith, W. R. Phillips, M. A. Jones, B. J. Varley, T. Rząca-Urban, I. Ahmad, L. R. Morss, M. Bentaleb, and N. Schulz, Nucl. Phys. A **689**, 605 (2001).

[11] W. Urban, T. Rząca-Urban, J. Wiśniewski, I. Ahmad, A. G. Smith, and G. S. Simpson, Phys. Rev. C **99**, 064325 (2019).

[12] W. Urban, T. Rząca-Urban, A. Złomaniec, G. Simpson, J. L. Durell, W. R. Phillips, A. G. Smith, B. J. Varley, I. Ahmad, and N. Schulz, Eur. Phys. J. A **16**, 11 (2003).

[13] J. K. Hwang, A. V. Ramayya, J. H. Hamilton, D. Fong, C. J. Beyer, P. M. Gore, Y. X. Luo, J. O. Rasmussen, S. C. Wu, I. Y. Lee, C. M. Folden, III, P. Fallon, P. Zielinski, K. E. Gregorich, A. O. Macchiavelli, M. A. Stoyer, S. J. Asztalos, T. N. Ginter, S. J. Zhu, J. D. Cole, G. M. Ter Akopian, Yu. Ts. Oganessian, and R. Donangelo, Phys. Rev. C **67**, 054304 (2003).

[14] W. Urban, J. A. Pinston, J. Genevey, T. Rząca-Urban, A. Złomaniec, G. Simpson, J. L. Durell, W. R. Phillips, A. G. Smith, B. J. Varley, I. Ahmad, and N. Schulz, Eur. Phys. J. A **22**, 241 (2004).

[15] A. Złomaniec, H. Faust, J. Genevey, J. A. Pinston, T. Rząca-Urban, G. S. Simpson, I. Tsekhanovich, and W. Urban, Phys. Rev. C **72**, 067302 (2005).

[16] P. J. Nolan, F. A. Beck, and D. B. Fossan, Annu. Rev. Nucl. Part. Sci. **44**, 561 (1994).

[17] I.-Y. Lee, Nucl. Phys. A **520**, c641 (1990).

[18] W. Urban, J. L. Durell, W. R. Phillips, A. G. Smith, M. A. Jones, I. Ahmad, A. R. Barnett, M. Bentaleb, S. J. Dorning, M. J. Leddy, E. Lubkiewicz, L. R. Morss, T. Rząca-Urban, R. A. Sareen, N. Schulz, and B. J. Varley, Z. Phys. A: Hadrons Nucl. **358**, 145 (1997).

[19] D. Patel, A. G. Smith, G. S. Simpson, R. M. Wall, J. F. Smith, O. J. Onakanmi, I. Ahmad, J. P. Greene, M. P. Carpenter, T. Lauritsen, C. J. Lister, R. F. Janssens, F. G. Kondev, D. Seweryniak, B. J. P. Gall, O. Dorveaux, and B. Roux, J. Phys. G **28**, 649 (2002).

[20] W. Urban, M. Czerwiński, J. Kurpeta, T. Rząca-Urban, J. Wiśniewski, T. Materna, L. W. Iskra, A. G. Smith, I. Ahmad, A. Blanc, H. Faust, U. Köster, M. Jentschel, P. Mutti, T. Soldner, G. S. Simpson, J. A. Pinston, G. de France, C. A. Ur, V.-V. Elomaa *et al.*, Phys. Rev. C **96**, 044333 (2017).

[21] I. Ahmad and W. R. Phillips, Rep. Prog. Phys. **58**, 1415 (1995).

[22] A. C. Wahl, At. Data Nucl. Data Tables **39**, 1 (1988).

[23] W. Urban, M. A. Jones, J. L. Durell, M. Leddy, W. R. Phillips, A. G. Smith, B. J. Varley, I. Ahmad, L. R. Morss, M. Bentaleb, E. Lubkiewicz, and N. Schulz, Nucl. Phys. A **613**, 107 (1997).

[24] H. Naidïdia, F. Nowacki, B. Bounthong, M. Czerwiński, T. Rząca-Urban, T. Rogiński, W. Urban, J. Wiśniewski, A. G. Smith, J. F. Smith, G. S. Simpson, I. Ahmad, and J. P. Greene, Phys. Rev. C **95**, 064303 (2017).

[25] S. J. Zhu, J. H. Hamilton, A. V. Ramayya, B. R. S. Babu, Q. H. Lu, W. C. Ma, T. N. Ginter, M. G. Wang, J. K. Deng, D. Shi, J. Kormicki, J. D. Cole *et al.*, J. Phys. G **21**, L75 (1995).

[26] J. L. Durell, Proc. Int. Conf. on Spectroscopy of Heavy Nuclei, Crete, Greece 1989, ed. J. F. Sharpey-Schafer and L. D. Skouras, IOP Conf. Series No. 105, p. 307.

[27] R. Licá, G. Benzoni, T. R. Rodriguez, M. J. G. Borge, L. M. Fraile, H. Mach, A. I. Morales, M. Madurga, C. O. Scotty, V. Vedia, H. De Witte, J. Benito, R. N. Bernard, T. Berry, A. Bracco, F. Camera, S. Ceruti, V. Charviakova, N. Cieplicka-Oryńczak *et al.*, Phys. Rev. C **97**, 024305 (2018).

[28] N. Pietralla and O. M. Gorbachenko, Phys. Rev. C **70**, 011304(R) (2004).

[29] K. Dusling and N. Pietralla, Phys. Rev. C **72**, 011303(R) (2005).

[30] Evaluated nuclear structure data file and experimental unevaluated nuclear data list of the Nuclear Data Center, Brookhaven National Laboratory, http://www.nndc.bnl.gov/2020

[31] E. Ideguchi, G. S. Simpson, R. Yokoyama, Mn. Tanaka, S. Nishimura, P. Doornenbal, G. Larusso, P.-A. Söderström, T. Sumikama, J. Wu, Z. Y. Xu *et al.*, Phys. Rev. C **94**, 064322 (2016).

[32] L. Gaudefroy, S. Péru, A. Arnal, J. Aupiais, J.-P. Delaroche, M. Girod, and J. Libert, Phys. Rev. C **97**, 064317 (2018).
[33] G. Andersson *et al.*, Nucl. Phys. A **268**, 205 (1976).
[34] B. R. Mottelson and S. G. Nilsson, Phys. Rev. **99**, 1615 (1955).
[35] P. Kleinheinz, Phys. Rev. Lett. **32**, 68 (1974).
[36] F. Barranco, G. F. Bertsch, R. A. Broglia, and E. Vigezzi, Nucl. Phys. A **512**, 253 (1990).
[37] R. A. Broglia, F. Barranco, G. F. Bertsch, and E. Vigezzi, Phys. Rev. C **49**, 552 (1994).
[38] K. Matsuyanagi, M. Matsuo, T. Nakatsukasa, K. Yoshida, N. Hinohara, and K. Sato, Phys. Scr. **91**, 063014 (2016).
[39] K. Heyde and J. L. Wood, Rev. Mod. Phys. **83**, 1467 (2011).
[40] P. E. Garrett, J. Phys. G **27**, R1 (2001).
[41] P. E. Garrett, W. D. Kulp, J. L. Wood, D. Bandyopadhyay, S. Choudry, D. Dashdorj, S. R. Lesher, M. T. McEllistrem, M. Mynk, J. N. Orce, and S. W. Yates, Phys. Rev. Lett. **103**, 062501 (2009).
[42] W. D. Kulp, J. L. Wood, K. S. Krane, J. Loats, P. Schmelzenbach, C. J. Stapels, R.-M. Larimer, and E. B. Norman, Phys. Rev. Lett. **91**, 102501 (2003).
[43] J. P. Schiffer, S. J. Freeman, J. A. Caggiano, C. Deibel, A. heinz, C.-L. Jiang, R. Lewis, A. Parikh, P. D. Parker, K. E. Rehm, S. Sinha, and J. S. Thomas, Phys. Rev. Lett. **92**, 162501 (2004).
[44] W. Urban, M. Saha Sarkar, S. Sarkar, T. Rząca-Urban, J. L. Durell, A. G. Smith, J. A. Genevey, J. A. Pinston, G. S. Simpson, and I. Ahmad, Eur. Phys. J. A **27**, 257 (2006).
[45] Y. X. Liu, C. J. Lv, Y. Sun, and F. Kondev, J. Phys. G **47**, 055108 (2020).
[46] Z. P. Li, T. Nikšić, D. Vretenar, J. Meng, G. A. Lalazissis, and P. Ring, Phys. Rev. C **79**, 054301 (2009).
[47] W. D. Kulp, J. L. Wood, P. E. Garrett, J. M. Almond, D. Cline, A. B. Hayes, H. Hua, K. S. Krane, R.-M. Larimer, J. Loats, E. B. Norman, P. Schmelzenbach, C. J. Stapels, R. Teng, and C. Y. Wu, Phys. Rev. C **71**, 041303(R) (2005).
[48] J. Dobaczewski, W. Nazarweicz, J. Skalski, and T. Werner, Phys. Rev. Lett. **60**, 2254 (1988).
[49] R. F. Casten, *Nuclear Structure from a Simple Perspective* (Oxford University Press, Oxford, 1990).
[50] W. Urban, T. Rząca-Urban, J. L. Durell, A. G. Smith, and I. Ahmad, Eur. Phys. J. A **24**, 161 (2005).
[51] R. Surman, J. Engel, J. R. Bennett, and B. S. Meyer, Phys. Rev. Lett. **79**, 1809 (1997).
[52] M. R. Mumpower, G. C. Mc Laughlin, and R. Surman, Phys. Rev. C **85**, 045801 (2012).
[53] J. Wu, S. Nishimura, G. Lorusso, P. Möller, E. Ideguchi, P.-H. Regan, G. S. Simpson, P.-A. Söderström, P. M. Walker, H. Watanabe, Z. Y. Xy *et al.*, Phys. Rev. Lett. **118**, 072701 (2017).